Earthquake Engineering, Tenth World Conference © 1992 Balkema, Rotterdam. ISBN 90 5410 060 5

Study on the applicability of a numerical analysis based on the effective stress theory

I. Kubodera, K. Itoh & Y. Goto
Technical Research Institute, Obayashi Corporation, Tokyo, Japan

ABSTRACT: This paper discuss the applicability of a computer code based on the effective stress theory by numerical analysing results of the dynamic centrifuge model tests which can reproduce a stress field comparable to that of real ground.

1 INTRODUCTION

Earthen embankments and semi-buried structures have been damaged due to soil liquefaction during past major earthquakes. The damage pattern of the earthen embankments (here after, "embankments") were demonstrated vertical or horizontal deformation due to liquefaction of the ground around it and semi-buried structures were damaged by heaving up. One of possible procedure to predict those deformations and to design countermeasures against them is a numerical analysis based on the effective stress theory. Up to now, many computer programs based on the effective stress theory have been developed by various agencies who then tried to apply them. Constitutive soil models have introduced on additional variable that must be taken into account in these programs and now these agencies are competing with each other to develop such programs.

Centrifuge testing is the best way to reproduce the stress-strain relationship of real ground, and the scaling relationship is concise compared to the model test in a 1 G field. Simulation of results of centrifuge test is one of the best method to verify the numerical procedure. Therefore, we conducted to verify the applicability of effective stress analysis code "DIANA-J2" using the dynamic centrifuge test which was conducted with the object of confirming the countermeasure against liquefaction for embankment and semi-buried structures. We also considered the behavior of embankments and semi-buried structures under soil liquefaction through this analysis.

2 ANALYSIS CODE AND OUTLINE OF THE ANALYSIS OBJECT

A computer code named "DIANA-J2" was used in this study. This code is based on the numerical formulation of the two-phase soil-water skeleton theory proposed by Biot. In the present study, we used u-U formulation where u represents the displacement of the soil, and U represents that of pore water. Also, we used the "Modified Multi-mechanism model" originated by Kabilamany and Ishihara which was modified by one of co-authors of the present study. The original Multi-mechanism model is an elasto-plastic constitutive model based on the non-associated flow rule. The plastic strain increment caused by principle stress axis rotation under a two-dimensional stress condition which was proposed by Matsuoka was introduced in the "Modified Multi-mechanism model".

Both models were evaluated for their abilities to simulate embankments and semi-buried structures deformation under liquefaction using the dynamic centrifuge test. Figures 1 and 2 show cross-sections of models, and Table 1 shows features of model materials. The ground material used in the test was Toyoura sand. The prototype ground consisted a 3～5m layer of saturated soft sandy ground ("Liquefiable Layer") which is susceptible to liquefaction, and a Compacted Layer. The countermeasure consists of cementing the ground around structure by the Deep Mixing Method using machinery to mix soil with hardening agents, such as lime and, on-site in order to strengthen the ground. Two types of tests were conducted. One of the improved model which is modeled by rigid body and one of a conventional model. Only the improved model was used for semi-buried structures.

3 RESULTS OF THE ANALYSIS

Table 2 shows the model parameters used in the analysis and Table 3 shows the physical properties of the model sand. Each model parameter was determined based on data given in previous papers on Toyoura sand. In these parmeters, hardening parameters a_m, a_c of the Liquefiable Layer ($D_r \fallingdotseq 60\%$) were determined from the simulation of undrained cyclic simple shear condition

which discribed in the reference. These values satisfy the condition which show liquefaction strength to be $\tau_{xy}/\sigma'_{mi}=0.15$ for the cyclic numbers $N_L=20$ in the undrained cyclic simple shear test. The values for the Compacted Layer ($D_r \fallingdotseq 100\%$) were less than those for the Liquefiable Layer and generated little excess pore water pressures.

3.1 Simulation of the undrained cyclic simple shear condition

Simulation of the undrained cyclic simple shear condition was conducted using the DIANA-J2 analysis code. Figure 3 shows the result of the Liquefiable Layer and Fig.4 shows that of the Compacted Layer. As seen in Fig.3, the effective stress path achieved cyclic mobility at almost $N_L=10$ and effective mean stress did not decrease any further thereafter. Though perfect liquefaction ($\sigma'_m=0$) was not reached, the excess pore pressure ratio generated was about 0.8. Therefore, we defined this condition as the perfect liquefaction. On the other hand, the effective mean stress decreased little even though the cyclic shear stress was applied, and it was concluded that the Compacted Layer did not liquefy (Fig.4).

3.2 Analysis of two-dimensional model including structure

Figures 5 and 6 show the finite element mesh of the centrifuge model. As boundary conditions, the side nodes of the mesh were placed on vertical rollers and the bottom nodes were fixed because rigid soil boxes were used in the centrifuge test. Using the rigid model, improved soil and semi-buried structures were shown to have stiffness equivalent to the test models (these models were also undrained). Before performing the dynamic analysis, initial stress analysis was carried out with boundary conditions equal to those used in the dynamic analysis. Although the model test with the conventional semi-buried structure model was not conducted, we analyzed the structure behavior without observing any improvement. The time increment for integral step was 2.5×10^{-5} seconds, and analysis was carried out through 0.25 seconds after the beginning of excitation (equivalent to 7.5 seconds of prototype).

3.2.1 Embakment model analysis

The conventional embankment model and the laterally improved embankment model are shown in Figs.7 and 8. These figures show the time histories of the excess pore water pressure of the Liquefiable Layer of the free field. Both the measured and calculated values achieved liquefaction and showed qualitative agreement. On the other hand, the calculated value of the conventional model showed an early rise in

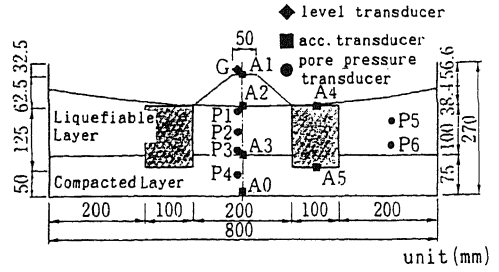

Fig.1 Laterally improved embankment model (centrifuge test)

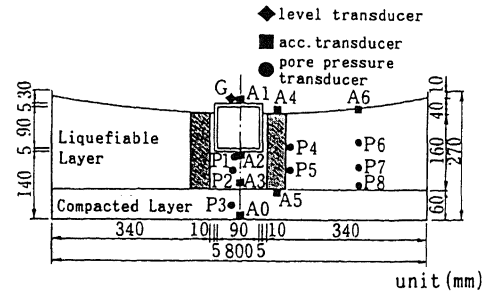

Fig.2 Laterally improved semi-buried structure model (centrifuge test)

Table 1 Summary of material data for the centrifuge test

Material	Properties	
Liquefiable Layer	Toyoura sand;	Relative density : $D_r \fallingdotseq 60\%$ Unit weight : $\gamma' \fallingdotseq 0.955 t/m^3$
Compacted Layer	Toyoura sand;	Relative density : $D_r \fallingdotseq 100\%$ Unit weight : $\gamma' \fallingdotseq 1.055 t/m^3$
Embankment	Mixture of kaolin clay and Toyoura Sand	Water content w=15% Unit weight $\rho \fallingdotseq 1.9 t/m^3$
Semi-buried Structure	Acrylic resin; Apparent specific gravity=1.7	
Improvement model	6mm thick steel plates Apparent specific gravity=1.9	
Pore water	30CS Silicon Oil; Density $\gamma' \fallingdotseq 0.955 t/m^3$	

Table 2 Model parameters

Items		Liquefiable Layer	Compacted Layer
Internal friction angle	ϕ_f	35°	37°
Dilatancy parameter	c	1.00	1.00
Stress ratio at phase transformation line	μ_{max}	1.20	1.20
Dilatancy parameter	S_c	0.0035	0.0035
Hardening parameter in the monotonic virgin loading	a_m	0.00006	0.000005
Hardening parameter in the cyclic loading	a_c	0.00006	0.000005
Slope of the compression curve	λ_c	0.0043	0.0008
Slope of the swelling curve	λ_s	0.0013	0.0002
Void ratio	e_0	0.760	0.593
Initial shear modulus	G_0	25,000kN/m²	34,000kN/m²
Mean stress at experiment	σ'_{ref}	98kN/m²	98kN/m²
Poisson's ratio	ν	0.33	0.33
Rotatinal angle	δ	30°	30°

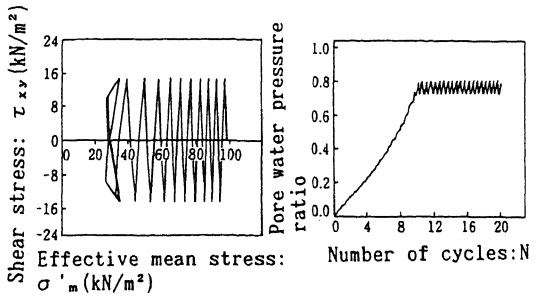

Fig.3 Effective stress path and pore pressure vs. cyclic numbers (Liquefiable Layer)

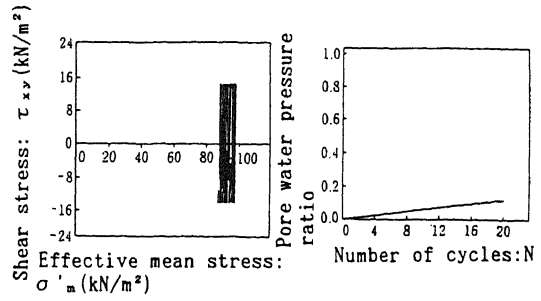

Fig.4 Effective stress path and pore pressure vs. cyclic numbers (Compacted Layer)

Table 3 Summary of the physical data of the materials

Items	; Soil skeleton	; Pore water
Bulk moduli	; K ; $1.\times10^{4}$ kN/m²	; 1.10×10^{6} kN/m²
Densities	; ρ ; 2.635t/m³	; 0.955t/m³
Rayleigh damping	; α ; 0.0	; 0.0
Rayleigh damping	; β ; 8.0×10^{-6}	; 0.0
Void ratio	; e ; 0.432	
Permeability	; k ;	; 5.0×10^{-5} m/sec

the excess pore water pressure and became disordered at 0.1 seconds in contrast with that of the improved model. Figures 9 and 10 show the direction of the principal stress during the initial stress analysis. The direction of the stress can be seen inside the circles in both figures. The values of conventional model tend to incline for the embankment compared to the improved model. Therefore, it can be said that the initial shears in the free field of the conventional model are larger than those of the improved model due to the weight of the embankment itself. Also the cause of disorder beginning at 0.1 seconds in the caluculation may be caused by the shear force from the deformation of the embankment and by the inherent analytical uncertainty in the program.

Figure 11 shows the time histories of the horizontal acceleration of the embankment in the conventional model. Figure 12 shows that of improved model. In Fig.11, measured and calculated values up to 0.1 seconds produced almost similar results, but after that a phase lag occured, which was almost equal quantitatively during maximum acceleration. In Fig.12, measured and calculated values up to 0.1 seconds produced similar results as well. Even though a phase lag occurred after 0.1 seconds, the improved model produced acceleration characteristics that were qualitatively similar since acceleration showed no further increase. A comparison of the measured and calculated values for horizontal acceleration of the embankment, revealed that there was no tendency toward amplification. Conversely, the results indicated horizontal similar stability characteristics, because the improved ground under the embankment had remained in good condition under excitation.

Figure 13 shows the time histories of

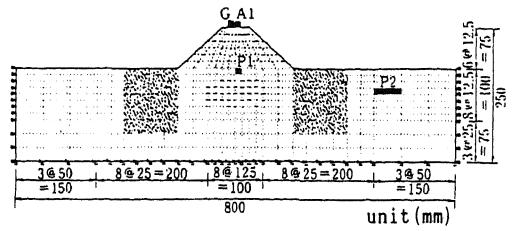

Fig.5 Analysis model (embankment model)

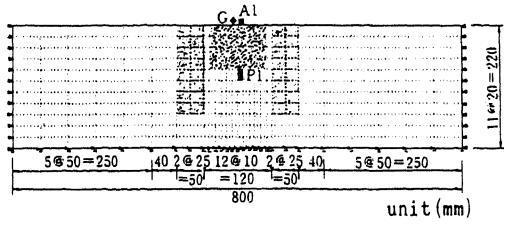

Fig.6 Analysis model (semi-buried structure model)

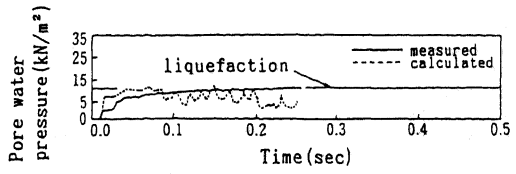

Fig.7 Measured and calculated excess pore water pressure at P2 (conventional embankment model)

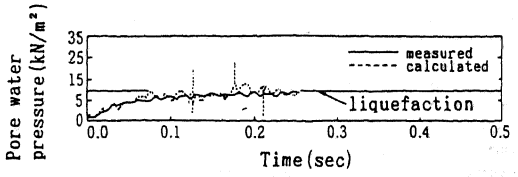

Fig.8 Measured and calculated excess pore water pressure at P2 (improved embankment model)

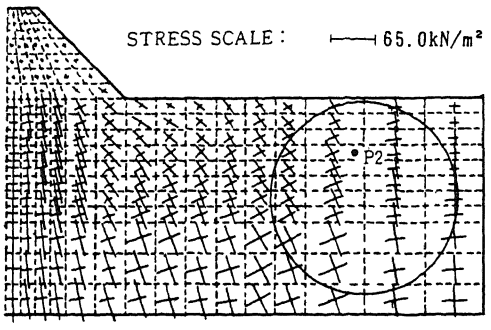

Fig.9 Direction of the principal stress of the initial stress analysis (conventional)

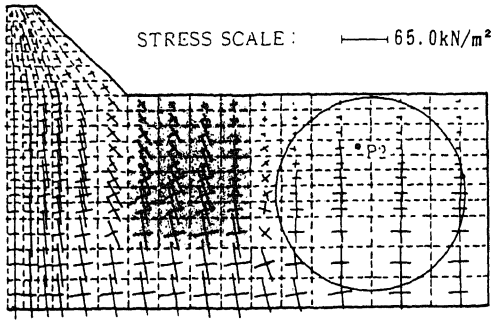

Fig.10 Direction of the principal stress of the initial stress analysis (improved)

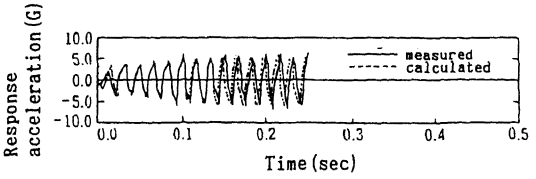

Fig.11 Measured and calculated response acceleration at A1 (conventional embankment model)

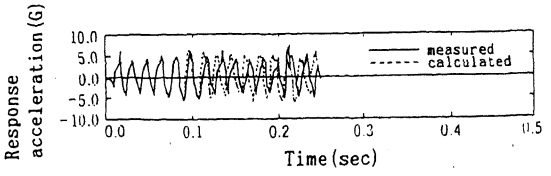

Fig.12 Measured and calculated response acceleration at A1 (improved embankment model)

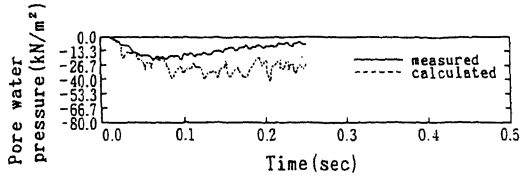

Fig.13 Measured and calculated excess pore water pressure at P1 (conventional embankment model)

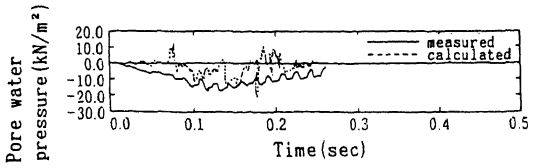

Fig.14 Measured and calculated excess pore water pressure at P1 (improved embankment model)

the excess pore water pressure at the Liquefiable Layer under the embankment of the conventional model and Fig.14 shows that of the improved model. As seen in Fig.13, measured and calculated values produced similar tendencies which showed negative pressure. Until nearly 0.1 seconds, they were almost completely in agreement, but after that the values became divergent. While the values in Fig.14 were not in agreement, there was a tendency for negative pressure to occur immediately after the beginning of excitation and then turned to positive pressure.

Figures 15 and 16 show that the time histories of both the measured and calculated values of crest settlement of embankments were in agreement qualitatively and quantitatively. These figures also demonstrate that the improved model produced less settlement than the conventional model.

Figures 17 and 18 show the deformation patterns of the two different embankment models over a period of 0.25 seconds. As seen in these figures, the DIANA-J2 code simulation showed that the improved ground prevented lateral deformation of both the embankment itself and of the ground under the embankment due to liquefaction of grounds on both sides of the embankments.

3.2.2 Analysis of semi-buried structures

The mechanism of uplift of semi-buried structures under soil liquefaction as described by Koseki, et al. are as follows:

① Uplift might be caused by the flow of the liquefied ground in the vicinity of the structure.

② Uplift might be caused by the unbalanced forces acting on the structure due to excess pore water pressure under the structure.

Uplift caused by term ① has been observed under shaking, and uplift caused by term ② has been observed principally after shaking. Since "DIANA-J2" is based on the minute deformation theory, it cannot simulate large permanent deformations. Therefore, the analysis performed was focused on initial permanent deformation caused by uplift.

Figure 19 shows the response acceleration of the semi-buried structures. The calculated value was almost twice as much as the measured value. This is because slides and separations which occur in the contact plane of the semi-buried structure and the ground around it were not considered in the analysis.

Figure 20 shows the time histories of

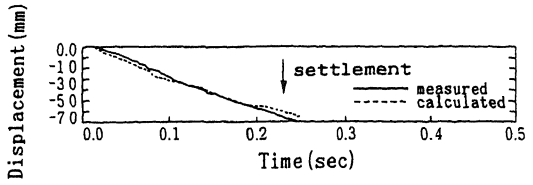

Fig.15 Measured and calculated crest settlement of embankment at G (conventional embankment model)

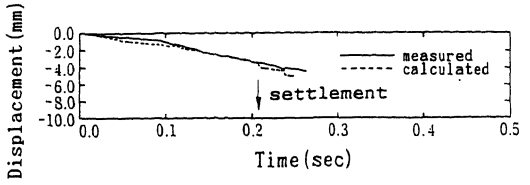

Fig.16 Measured and calculated crest settlement of embankment at G (improved embankment model)

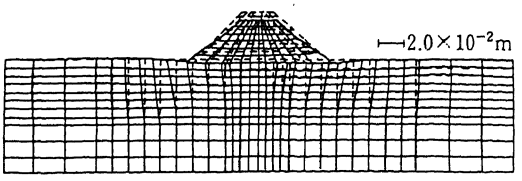

Fig.17 Calculated deformation pattern at 0.25 sec after shaking (conventional embankment model)

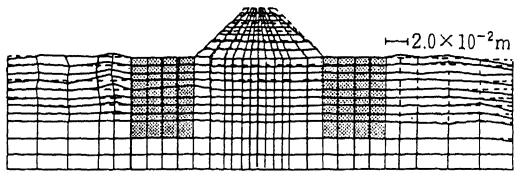

Fig.18 Calculated deformation pattern at 0.25 sec after shaking (improved embankment model)

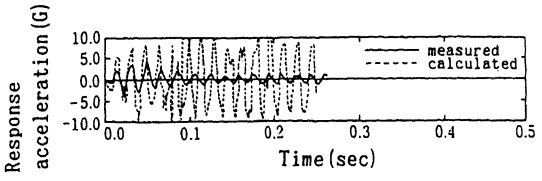

Fig.19 Measured and calculated response acceleration at A1 (improved semi-buried structure model)

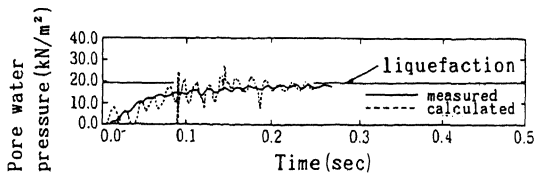

Fig.20 Measured and calculated excess pore water pressure at P1 (improved semi-buried structure model)

the excess pore water pressure in the Liquefiable Layer under the semi-buried structure. The results in this figure indicated that the ground under the semi-buried structure liquefied. The increase in the excess pore water pressure values were consistent.

Figure 21 shows the vertical displacement of semi-buried structure in the improved model. Figure 22 shows the deformation patterns over a period of 0.25 seconds. The results of the conventional model in Figs.21 and 22 were consistent.

As seen in Figs.21 and 22, in spite of liquefying the ground under the semi-buried structure, almost no heaving up occured. The results shown in Fig.23 indicated that semi-buried structure heaved up immediately following excitation when using the conventional model.

3.2.3 Analysis of semi-buried structures including the joint element

Analysis of the measured and the calculated values of semi-buried structures produced very different results in terms of acceleration of the semi-buried structure. Therefore, the improved model which included the joint element in the contact plane between the semi-buried structure and the ground around it was analyzed again. Table 4 shows the parameters of the joint element.

Figure 25 shows the response acceleration of the semi-buried structure and Fig.26 shows the variation of uplift over time. As seen in Fig.25, it well analyzed better than that of Fig.19 especially in the tendency of decreasing the response. Then, from Fig.26, we can see that the calculated displacement of semi-buried structures were different from the experimental results. Theoretically, heaving up began at the moment shaking started, however, it was only 0.25 mm for a period of 0.25 seconds and the difference between the measured and the calculated values was only about 0.3 mm. This amount of heaving up was smaller than that of the analysis without the joint element which produced about 1.0 mm. Therefore, it can be said that the amount of uplift of semi-buried structure was negligible. As seen in the variation over time of the measured results, sink was first observed, followed by heave and then sink again. The first sink phase probable occured as a result of the semi-buried structure model setting into the ground around it. This phenomenon is peculiar to this examination. Therefore, due to the discrepancies between calculated and measured results, it is impossible to simulate this phenomenon using numerical analysis.

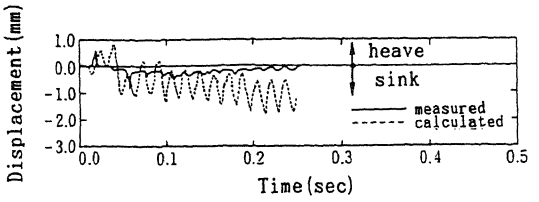

Fig.21 Vertical displacement of semi-buried structure at G (improved semi-buried structure model)

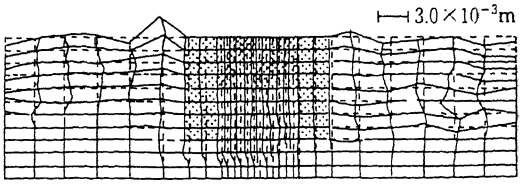

Fig.22 Calculated deformation pattern at 0.25 sec after shaking (improved semi-buried structure model)

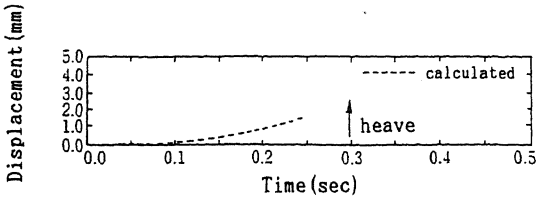

Fig.23 Vertical displacement of semi-buried structure at G (conventional semi-buried structure model)

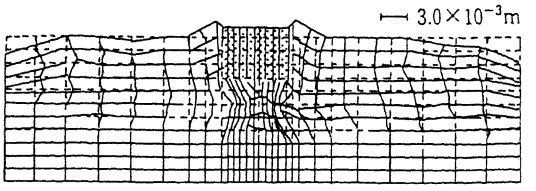

Fig.24 Calculated deformation pattern at 0.25 sec after shaking (conventional semi-buried structure model)

Table 4 Joint element parameters

Friction angle	: ϕ_J	: 30°
Cohesion	: C	: 0
Shear spring	: k_s	: 4.3×10^3 kN/m²
Vertical spring	: k_n	: 1.69×10^4 kN/m²
Poisson's ratio	: ν	: 0.3
Modulus of elasticity	: E	: 2.68×10^4 kN/m²

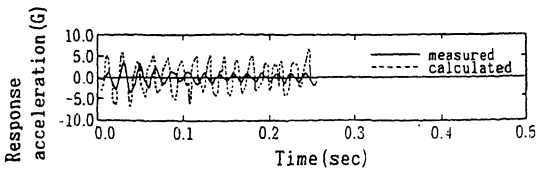

Fig.25 Measured and calculated response acceleration at A1 (improved semi-buried structure model with joint element)

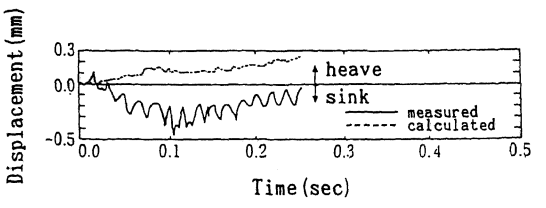

Fig.26 Vertical displacement of semi-buried structure at G (improved semi-buried strucure model with joint element)

4 CONCLUSIONS

The proposed numerical analysis code based on the effective stress theory successfully analyzed the qualitative aspects, and to a lesser extent quantitative aspects, of deformations induced by soil liquefaction of embankments and semi-buried structures.

Through the numerical simulation, ground improvement on both sides of the structure was shown to be effective in preventing the lateral flow of the ground and in decreasing the settlement or heaving of structures in or on the liquefiable ground.

More improvements such as stability of analysis and shortening calculation time will be required to increase the practical applications of this code.

5 ACKNOWLEDGEMENTS

The dynamic centrifuge test used to test the numerical simulations was conducted at the Public Works Research Institute, Ministry of Construction ("P.W.R.I"), Japan on the P.W.R.I. 2 m Dynamic Centrifuge. The tests were conducted jointly by P.W.R.I., Takenaka Corp., Fudo Const. Co. Ltd, Takenaka civil Eng. and Const. Co. Ltd, and Obayashi Corp. The authors would like to express their thanks to all of these organizations.

REFERENCES

Kabilamany, K. and Ishihara, K. 1988. Stress dilatancy and hardening laws for rigid granular model of sand. Soil Dynamics and Earthquake Engineering.

Koga, Y. et al. 1991. Applicability of the dynamic centrifuge model test method in developing countermeasures against soil liquefaction. CENTRIFUGE 91:431-438

Koseki, J. et al. 1990. Uplift of Semi-buried Structures in Liquefiable Sands during Earthquake. Proceedings of The Eighth Japan Eathquake Engineering Symposium:933-938